Compact EBG-Backed Planar Monopole for BAN Wearable Applications

M. Ali Babar Abbasi *Student Member IEEE*, Symeon Nikolaou *Member IEEE*, Marco A. Antoniades *Member IEEE*, Marija Nikolic *Member IEEE*, Photos Vryonides *Member IEEE*

***Abstract*— This paper presents a planar monopole backed with a 2×1 array of Electromagnetic Band Gap (EBG) structures. The reflection phase of a single EBG unit cell has been studied and exploited towards efficient radiation of a planar monopole antenna, intended for wearable applications. The shape of the EBG unit cell and the gap between the ground and the EBG layer are adjusted so that the antenna operates at 2.45 GHz. The proposed antenna retains its impedance matching when placed directly upon a living human subject with an impedance bandwidth of 5%, while it exhibits a measured gain of 6.88 dBi. A novel equivalent array model is presented to qualitatively explain the reported radiation mechanism of the EBG-backed monopole. The proposed antenna is fabricated on a 68×38×1.57 mm^3 board of semi-flexible RT/duroid 5880 substrate. Detailed analysis and measurements are presented for various cases when the antenna is subjected to structural deformation and human body loading, and in all cases the EBG-backed monopole antenna retains its high performance. The reported efficient and robust radiation performance with very low specific absorption rate (SAR), the compact size, and the high gain, make the proposed antenna a superior candidate for most wearable applications used for off-body communication.**

***Index Terms*—Electromagnetic band gap, planar monopole, wearable, antenna, biomedical**

I. Introduction

With the rapid development in communication systems in the past few years, the area of wireless body area networks (WBAN) has grown significantly, supporting a large number of applications, including personalized health care systems, patient monitoring systems, rescue systems, battle field survival, and wearable gaming consoles [1-2]. Several frequency bands have been allocated for these applications to commercialize WBAN communication systems, which include the Medical Implantable Communication Systems (MICS) band (402-405 MHz), Industrial Scientific and Medical (ISM) band (2.40-2.48 GHz) and Ultra Wideband (UWB). For optimum performance, the antennas used for WBAN applications are required to be compact, mechanically robust, lightweight and preferably comfortable while being worn. It has been reported, that the performance of an antenna may degrade significantly while operating in close proximity with the human body [1-2]. This occurs because the antenna's surface currents are affected by the near field coupling with the body, which in turn affects the input impedance matching of the antenna. Specifically, for narrow-band operation, the dominant effect of the body proximity is a shift of the resonance frequency, which causes a mismatch at the designed frequency, resulting in a significant degradation of the total efficiency ($P_{radiated}/P_{incident}$). Designing a narrowband wearable antenna with a high total efficiency can be a challenging task, especially when it is also expected for the antenna to have low-profile, conformal and lightweight characteristics [2]. At the same time, the effect of wearable antennas on the human body in terms of maximum allowable specific absorption rate (SAR) needs to be addressed [3]. So far a number of configurations have been investigated as potential candidates for wearable antennas including fractal [4], inverted-F [5], planar monopoles [6-8], magneto electric dipoles [9], cavity backed [10, 11], and stacked microstrip antennas [12].

The microstrip antenna presented in [12], and the cavity backed antennas [10-11], can be considered good potential candidates for wearable applications, however they do not exhibit conformal characteristics. Several textile-based conformal antennas, including a wearable magneto electric dipole [9], a fully grounded microstrip [13], textile fractal [4] and textile antenna based on Substrate-Integrated Waveguide (SIW) technology [14] are proposed to be pliable for off-body communication, however they have a relatively large footprint. A recent investigation on a compact conformal inverted-F wearable antenna has been presented [5]; however, due to its near-omnidirectional radiation properties, a significant amount of energy is directed towards the human body. In an attempt to direct the antenna radiation away from the body for off-body communication with a BAN base station like the one presented in [15], it is always desirable to have a full ground plane. The presence of a ground plane also increases the isolation between the wearable antenna and the body, thus resulting in lower SAR values [16]. Other than conventional full or extended ground planes [12-13, 17-19], periodically loaded configurations using high impedance surfaces [20-21], artificial magnetic conductors and electromagnetic/photonic band gap structures [6-7, 20, 22-24] have been investigated to introduce improved isolation between the radiating wearable antenna and living human tissues. However, these configurations still suffer from frequency shifts due to either bending, or crumpling, or they have relatively large lateral sizes.

In this paper, we present the novel design of a very

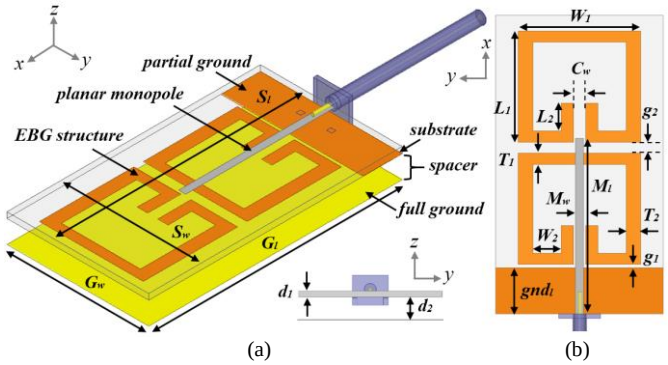

Fig. 1. (a) Configuration of the 2×1 EBG-backed planar monopole antenna with full ground (b) Top view of the monopole and finite sized EBG layer. Antenna is fabricated on semi flexible Rogers RT/duroid 5880 substrate with ε_r = 2.2 and $tan\delta$ = 0.0009.

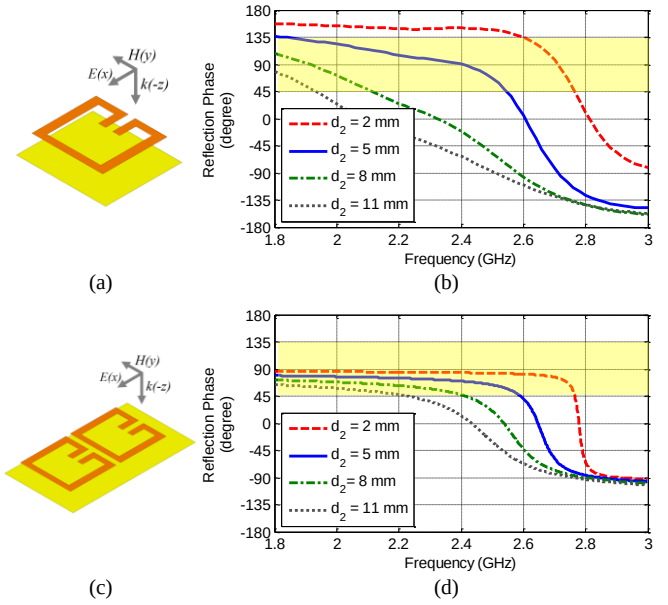

Fig. 2. (a) Configuration of a single unit cell consisting of the EBG element with metallic backing under plane wave excitation. (b) Reflection phase of an infinite array of the EBG unit cells. (c) Configuration of a 2×1 array of EBG cells under plane wave excitation (d) Reflection phase of the 2×1 array of EBG cells.

compact EBG-backed planar monopole antenna and the experimental realization of a conformal low-profile wearable antenna operating at 2.45 GHz in the ISM band. It is worth mentioning here that contrary to recently reported wearable antennas operating in the UHF [16, 20], ultra wideband (UWB) [12-13, 17] and super wideband [4] frequency bands, this paper primarily focuses on the implementation, of a low profile, conformal, highly efficient, narrowband wearable antenna for off-body communication in wireless body area networks. The proposed antenna shown in Fig. 1 consists of a radiating monopole, backed by a very compact 2×1 cell EBG structure exhibiting controllable reflection phase, which radiates with high directivity and high efficiency even when it operates adjacent to living human body. The finite size ground plane provides high isolation between the antenna and the living human body tissues beneath it. At the same time, the

TABLE I
DIMENSIONS OF THE EBG-BACKED PLANAR MONOPOLE OF FIG. 1

parameter	Length (mm)	parameter	Length (mm)
S_w	38.00	W_1	27.83
S_l	68.00	W_2	06.40
G_w	38.00	L_1	25.30
G_l	68.00	L_2	06.32
d_1	01.57	M_l	40.00
d_2	05.00	M_w	01.80
T_1	02.53	g_1	00.75
T_2	03.34	g_2	02.50
C_w	02.78	gnd_l	10.50

ground plane in combination with the radiating monopole backed with an EBG surface contributes towards significantly higher gain compared to conventional planar monopole antennas. The antenna design details are presented in section II with a novel array model that provides a qualitative explanation of the radiation mechanism, while section III presents the experimental results of the fabricated prototype. Finally, section IV presents the performance of the antenna when it is subjected to structural deformation and placed on a human body.

II. ANTENNA DESIGN

A. Antenna Configuration and EBG Structure Selection

The antenna schematic shown in Fig. 1 consists of a radiating monopole, backed by a 2×1 array of EBG cells. The top planar monopole and the partial ground plane are printed on the opposite sides of a substrate making a standalone planar monopole antenna. A customized EBG structure is printed on the same side of the substrate where the partial ground plane is printed to form an EBG surface, hence utilizing the available space and reducing the overall size of the antenna. The full ground plane beneath the EBG structure is separated by a thin foam spacer.

At the initial design stage, the EBG structure has been designed so that the surface wave frequency bandgap of the EBG layer overlaps the matched frequency band of the planar monopole, to form a combined operating frequency band for the antenna. The EBG unit cell consists of a compact split squared ring resonator with an elongated length L_2 and a coupling gap C_w between the two symmetrical parts of the structure [25]. The EBG structure is symmetric along the *x*-axis as shown in Fig. 1(b) and 2(a). The adapted shape of the single EBG cell [26] and the air gap between the EBG layer and the ground plane depict built-in anisotropic behavior, having a strong LC resonance along the *x*-axis [27]. This implies that the EBG structure exhibits a different electric response for a wave polarized parallel to the *x*-axis as compared to a wave polarized parallel to the *y*-axis, when the wave is propagating along the *z*-axis. Ansoft HFSS, based on the finite element method (FEM), is used to simulate the electromagnetic response of the EBG structure. Fig. 2(b) shows the reflection coefficient phase when a single EBG unit cell is illuminated with a linearly polarized plane wave that is polarized along the *x*-axis. The reference plane has been de-

embedded up to the point where the linearly polarized planar monopole will be located. The structural parameters of the EBG structure, namely, L_1, L_2, W_1, W_2, T_1, T_2 and C_w were optimized to define the EBG surface wave frequency band gap. The designated reflection phase for the EBG structure operation agrees well with the work presented in [28-29], which argues that it is advantageous in terms of the antenna impedance matching to work in the region where the reflection phase of the EBG plane is $90°\pm45°$. The defining parameter for this $90°\pm45°$ bandwidth is the gap between EBG structure and ground plane (d_2) which provides direct control over the reflection phase of the EBG structure (see Fig. 2(b)). In [28] it was also concluded that the operational EBG bandwidth increases as the contour of the reflection phase in the transition region becomes smoother, a characteristic that also depends on the parameter d_2.

B. Antenna Miniaturization

The work presented in [7] describes an inkjet printed planar monopole backed by a 4×3 array of similar planar split ring structures [26] operating at a $\sim0°$ phase reflection bandwidth namely at the Artificial Magnetic Conductor (AMC) band. The dimensions of the antenna in [7] are rather large for wearable applications. Also, the use of a paper substrate further decreases the robustness of the antenna in adverse environmental conditions. These seemingly disadvantageous characteristics motivated the design and miniaturization of an EBG array backing a printed monopole, on a more robust and semi-flexible substrate. In this section, the miniaturization from a 4×3 to 2×1 EBG array is discussed stepwise in order to obtain some engineering design guidelines. The miniaturization presented in Fig. 3 and summarized in Table. II consists of the following steps:

Step 1: A radiating monopole backed by a 4×3 EBG array was designed on a Rogers RT/duroid 5880. Note that the ground plane, backing the EBG structure, was reduced to 125×96 mm^2 compared to 150×120 mm^2 in [7], hence decreasing the overall footprint of the antenna at this initial design phase. The reflection coefficient and radiation efficiency of a planar monopole backed with 4×3 EBG array is mainly determined by three parameters (see Fig. 1): the monopole length (M_l), the monopole width (M_w) and the gap between the monopole and the bottom ground plane (d_2). The EBG reflection phase band (controlled primarily by d_2) was matched with the resonance of the planar monopole by optimizing the parameters M_l and M_w. The optimized reflection coefficient of the 4×3 EBG-backed monopole is presented in Fig. 3(b) whereas the optimized parameters and results are listed in Table II.

Step 2: Since most of the radiating fields reside in the center of the 4×3 EBG array, the array matrix was decreased from 4×3 to 3×2, targeting a ~50% size reduction. The initial reflection coefficient was poor in the ISM band, but it was subsequently optimized so that the antenna radiated at a higher efficiency. The noticeable effect of this miniaturization was the small decrease in the peak gain of the antenna, from 9.78 dBi to 8.97 dBi, when the array size was reduced from 4×3 to 3×2.

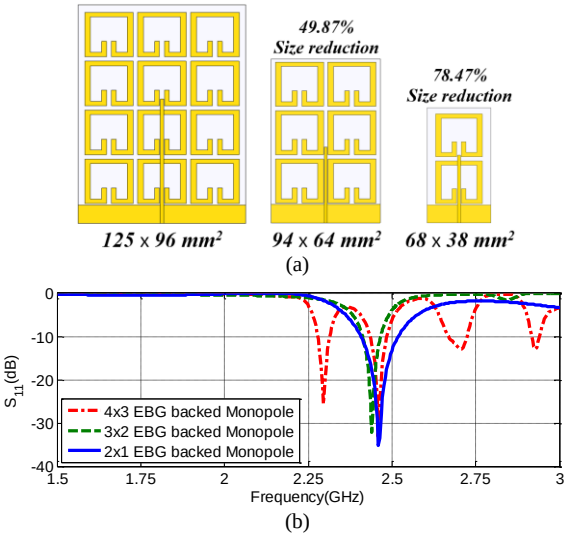

Fig. 3. Miniaturization of antenna (a) steps with the percentage size reduction (b) Reflection coefficient when the antenna is optimized in the 2.45 GHz ISM band.

TABLE II
SUMMARY OF MINIATURIZATION

	Step 1	Step 2	Step 3
Optimized dimensions of parameters (mm)			
S_w	96.00	64.00	38.00
S_l	125.00	94.00	68.00
d_2	03.25	04.00	06.00
M_l	70.50	43.50	40.00
M_w	03.80	01.60	01.80
Optimized results			
Reflection Coefficient	-32 dB	-31 dB	-34 dB
Bandwidth	2.43-2.48 GHz	2.41-2.46 GHz	2.40-2.52 GHz
Radiation Efficiency	95%	96%	76%
Gain Max.	9.78 dBi	8.97 dBi	6.88 dBi

Step 3: Based on the same observation of weak radiating fields along the edges of the antenna, miniaturization from a 3×2 to a 2×1 EBG array was achieved. Re-optimization of the antenna dimensions led to the set of parameters listed in Table II that resulted in efficient radiation of the antenna in the ISM band, from 2.40 – 2.52 GHz, with a gain of 6.88 dBi at 2.45 GHz. The final proposed structure, from Step 3, shows a significant size reduction of the proposed antenna, compared to previously reported EBG- and AMC-backed designs [6- 7, 21-24, 30-31].

C. Parametric analysis

The simulated and measured reflection coefficient of the fabricated 2×1 EBG-backed monopole is shown in Fig. 4(a). The $90°\pm45°$ phase bandwidth available for the operation of the optimized EBG layer is considerably wider than the S_{11} < -10 dB bandwidth of a conventional planar monopole. To further appreciate this point, let us observe the effect of gap d_2 on the reflection phase in Fig. 2(d) compared to the effect on the reflection coefficient in Fig. 4(b). It is evident that, the input impedance frequency band overlaps with the surface-

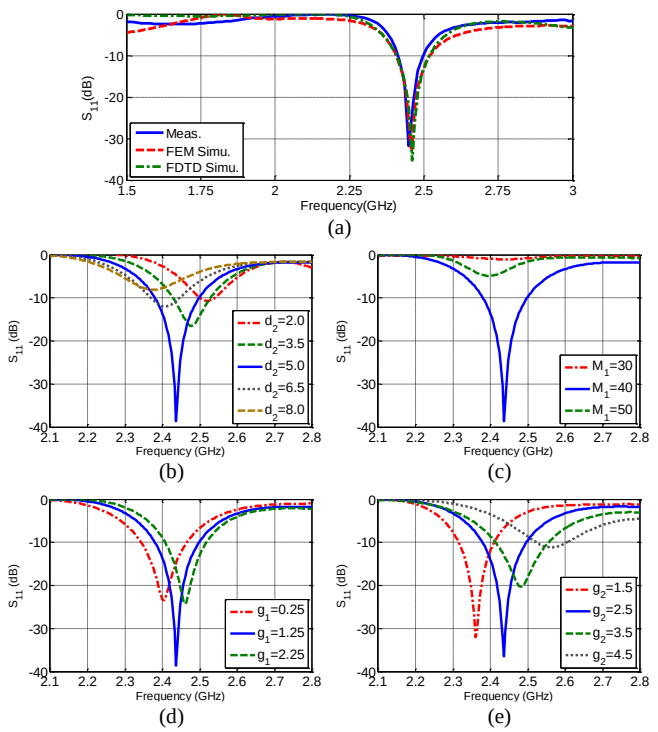

Fig. 4. (a) Comparison of 2×1-EBG-backed monopole measured S_{11} with simulated S_{11} using finite element method (FEM) and simulated using finite difference time domain method (FDTD). Parametric study of: (b) monopole length M_1, (c) gap between EBG and ground plane d_2 (d) gap between RF ground and first EBG cell g_1 and (e) gap between EBG cells g_2 all in mm.

wave frequency band of the EBG structure for a wide range of d_2 values (i.e. around 3 mm). This operation also corroborates the theoretical studies presented in [28, 32]. This fact makes the proposed antenna rather robust and immune to gap size (d_2) changes, and as a result its operation is not significantly disturbed when the gap is perturbed. This robustness feature is always desirable for a wearable antenna because it is often subjected to mechanical stress, which would tend to change the value of d_2. The length of the planar monopole (M_1) significantly affects the impedance matching of the antenna, whereas, the gap g_1 controls the resonance frequency of the antenna as shown in Fig. 4(c) and (d) respectively. The variation of the gap between two consecutive EBG cells, g_2, affects both the impedance matching and the antenna resonance frequency and is the most sensitive design parameter. As the g_2 increases, the frequency resonance shifts towards higher frequencies as reported also in [28].

III. Radiation Characteristics

A. Radiation performance and mechanism

The proposed antenna has the maximum directivity along the positive *z*-axis as shown in Fig. 5. The main radiation lobe has a *94*° and *62*° half-power beam width (HPBW) in the *y*-*z* plane and *x*-*z* plane, respectively. The radiation pattern depicts relatively low radiation in the backward direction, at the location of human tissue when the antenna is placed directly on the human body. This factor also decreases the maximum

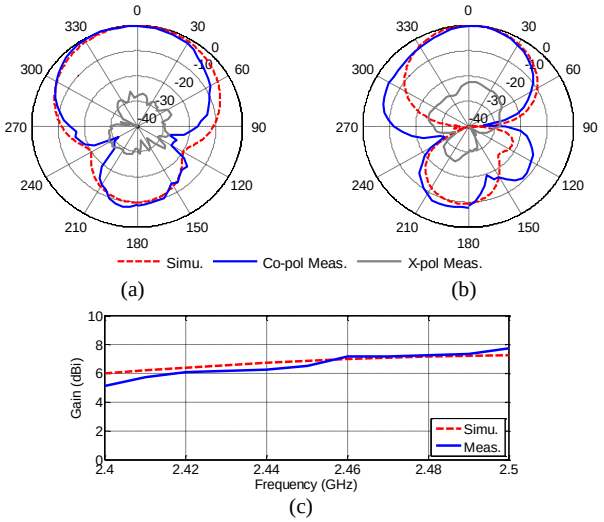

Fig. 5 Simulated and measured (a) *y*-*z* plane and (b) *x*-*z* plane normalized radiation patterns of the 2×1 EBG-backed monopole antenna at 2.45 GHz. (c) Simulated and measured peak gain of the 2×1 EBG-backed monopole

SAR value of the antenna which is a desired characteristic for any wearable antenna. The directional radiation patterns of the proposed antenna are caused not only by the electric monopole but also by the surface currents induced on the metallic surface of the EBG structure, placed over a full ground plane that creates an array of slots. These slots can be modeled as equivalent magnetic current sources, which form a centrally-excited 3×1 array. To further elaborate on this, the electric field plotted on the substrate directly beneath the EBG surface is presented in Fig. 6(a), where the locations of the equivalent magnetic current sources are identified in dotted rectangles. These radiating slots can be replicated by placing three independent magnetic current sources ($\overrightarrow{M_1}, \overrightarrow{M_2}, \overrightarrow{M_3}$) at the same location. Considering the combined effect of the ground plane and the EBG layer, it can be assumed that the resultant radiation pattern is radiated by a virtual eight-element array as shown in Fig. 6(b). The eight-element array consists of 2x1 elements excited by electric current sources and 3x2 elements excited by magnetic current sources. In Fig. 6, $\overrightarrow{M_1}, \overrightarrow{M_2}$ and $\overrightarrow{M_3}$ represent the independent magnetic current sources, while $\overrightarrow{M_1'}, \overrightarrow{M_2'}$ and $\overrightarrow{M_3'}$ indicate their images upon reflection on the metasurface that causes a 90° phase difference between the radiating elements and their images. Similarly, $\vec{I}$ represents the electric current on the planar monopole and $\vec{I'}$ represents its image. For the analysis, the current on each element is expressed in complex form: $A_1 e^{j\psi_1}$,$A_2 e^{j\psi_1}$, $A_3 e^{j\psi_1}$, $A_1 e^{j\psi_2}$, $A_2 e^{j\psi_2}$, $A_3 e^{j\psi_2}$, $Be^{j\psi_1}$ and $Be^{j\psi_2}$, where A_1, A_2, A_3 and B represent the magnitudes of each current source and ψ_1 and ψ_2 represent the phases of the real and image sources, respectively. The magnitude excitations A_i and B can be approximated from the simulated electric field distribution presented in Fig. 6(c) and are normalized with respect to the maximum value A_2. Based on the same distribution, the normalized value of the electric current magnitude is $B = 1.00$ and the estimated relative magnetic current magnitudes are $A_1 = 0.65$, $A_2 = 1.00$ and $A_3 = 0.55$. Based on the time domain animation of the *E*-field distribution they radiate in phase with each other. Hence, all three magnetic current

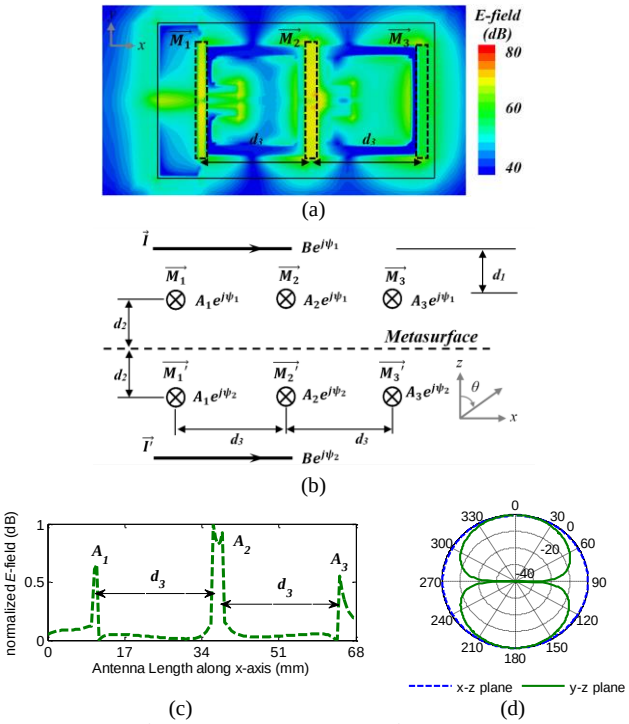

(a) (b) (c) (d)

Fig. 6. (a) Electric field distribution on EBG surface depicting three magnetic current sources ($\overrightarrow{M_1}, \overrightarrow{M_2}, \overrightarrow{M_3}$) at 2.45 GHz, (b) Equivalent eight-element array model consisting of two electric current sources and six magnetic current sources, (c) Simulated electric field on the EBG layer along the *x*-axis, which is used to model the magnitude of the magnetic current sources, (d) Simulated electric field pattern of a ~λ/4 magnetic current source.

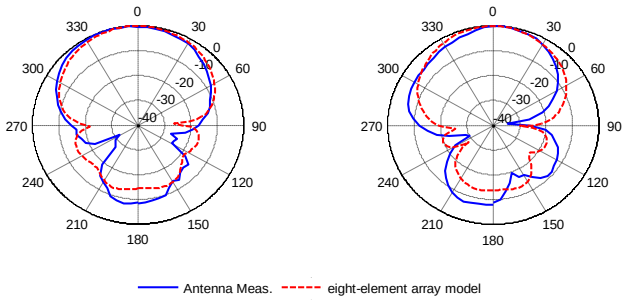

(a) (b)

Fig. 7. Electric field patterns comparison between of 2×1 EBG-backed monopole antenna and the eight-element array model (a) along the *y*-*z* axis and (c) along the *x*-*z* axis.

sources above the metasurface have the same phase, ψ_1, while the image sources below the metasurface have a phase of ψ_2. As explained in Section II.A and Fig. 2(b), the reflection phase exhibited by the grounded EBG metasurface is selected to be *90°*, meaning that the phase difference between ψ_1 and ψ_2 is *90°* as well. It is known that the total electric field of multiple independent radiating elements is equal to the product of the field of a single source and the array factor, so the behavior of the six-element array is determined by the array factor for six magnetic current sources given by:

$$AF_M = AF_h \times AF_v \tag{1}$$

Here, AF_h is the array factor for the three-element magnetic current sources distributed along *x*-axis, and AF_v is the array factor for the two sets of three-element linear arrays, distributed along the *z*-axis. The six magnetic currents which are aligned along the *y*-axis have omni-directional radiation patterns along the *x*-*z* plane and are linearly polarized with an E_φ component (assuming that the magnetic currents are oriented parallel with the *z*-axis) to be the dominant polarization. The electric field derived for a magnetic current source is presented in [33]:

$$E(\theta) \cong -j\frac{M_o e^{-jkr}}{2\pi r}\frac{\cos\left(\frac{kl}{2}\cos\theta\right)-\cos\left(\frac{kl}{2}\right)}{\sin\theta} \tag{2}$$

Where k is the wavenumber, r is the distance from the source centre, and M_o is the amplitude of the magnetic current excitation. Considering the "global" axes presented in Fig. 6(b), this coincides with the E_θ polarization. The polarization of the radiated field is in agreement with the measured co-polarization. However, for the calculation of the *E*-field along the *y*-*z* plane, the normalized distribution of the individual magnetic currents has to be considered. The normalized array factor pattern is calculated for an arrangement replicating the radiating mechanism of the proposed 2×1 EBG-backed monopole, where, d_2 = 5.8 mm (~λ/20) and d_3 = 26.7 mm (~λ/4). The calculated array factor for the magnetic current sources, AF_M, is then superimposed with the radiation pattern of the remaining 2×1 monopole elements represented by $\vec{I}$ and $\vec{I'}$ to form a radiation pattern for an eight-element array model. It should be noted that despite the fact that the orientation of the 2×1 electric currents is orthogonal with the orientation of the 3×2 magnetic currents, their dominant radiated *E*-field polarization coincides because they are excited by electric and magnetic sources respectively. In both Figs 7(a) and (b), the solid lines show the co-polarized measured radiation patterns of the 2×1 EBG-backed monopole, whereas the dotted lines show the calculated *E*-field pattern of the combined eight-element current source array model. The location of the nulls in Fig. 7(a) for the eight-element model is exactly at *90°* and *270°*, which do not coincide exactly with the nulls in the measured radiation pattern (blue solid contour). This discrepancy is mostly because of the approximation of the limited size ground plane $G_l \times G_w$ with an ideal infinite ground plane for the eight-element array. Other than the slight relocation of nulls, it can be observed that the suggested radiation mechanism of the eight-element array is in very good agreement with the measured radiation patterns of the fabricated 2×1 EBG-backed monopole. This verifies the validity of the presented eight-element array model presented in Fig. 6(b) and also demonstrates the effect of the metasurface that causes the intended *90°* phase difference between the physical radiators and their images.

IV. Experimental Results

The 2×1 EBG-backed monopole was fabricated on an LPKF ProtoMat H 100 milling machine. Styrofoam with the prescribed thickness was added as a spacer between the EBG layer and the finite ground plane (Fig. 8). An Agilent E8363B network analyzer was used to characterize the reflection coefficient of the antenna in free space. As shown in Fig. 4(a), good agreement can be seen between measurements and simulated predictions not only in terms of resonance position, but also with respect to the 10 dB bandwidth. The measured

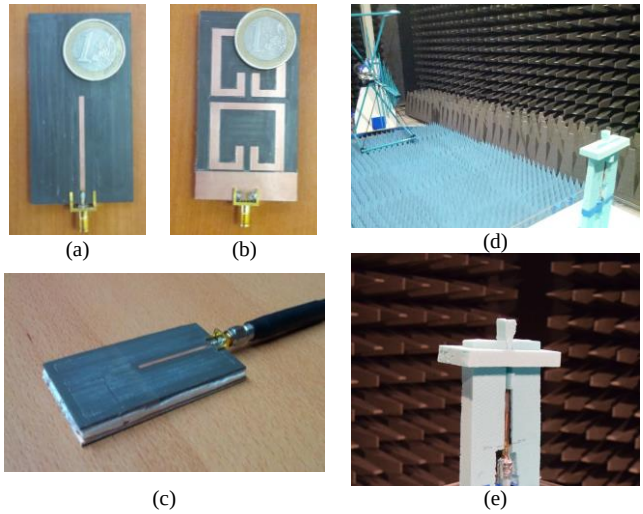

Fig. 8. Photographs of the fabricated antenna (a) on the planar monopole side (front side) (b) on the 2×1 EBG plane side (back side) (c) assembled integrated antenna connected to a VNA (d) Radiation pattern measurement setup in an anechoic chamber and (e) antenna supported by low-loss Styrofoam over a rotating platform connected to an SMA connector and a balun in the anechoic chamber.

reflection coefficient of the 2×1 EBG-backed monopole antenna has a -10 dB bandwidth ranging from 2.40 to 2.50 GHz, which is slightly narrower than the simulated response. This small discrepancy between the measurement and simulation can be related to the additional Ohmic losses normally generated while soldering the SMA connector on the fabricated prototype.

The measured co-polarized and cross-polarized radiation patterns compared to the simulations are shown in Fig. 5. The measurements were taken in an anechoic chamber at the Idvorski Laboratories Serbia, co-owned by the School of Electrical Engineering, University of Belgrade. The antenna was placed on an automatic rotating platform (Fig. 8(d) and (e)) and gain patterns were measured at 11 discrete frequency points from 2.4 to 2.5 GHz as shown in Fig. 5(c). Simulation and measurements are in good agreement. It can be observed that the antenna retains a reasonable directional radiation pattern in the +*z* hemisphere, confirming the simulation predictions. In the *x*-*z* plane radiation pattern, the measured HPBW agrees well with the simulated predictions, which is around *93*°. In the *y*-*z* plane radiation pattern, the measured HPBW of the 2×1 EBG-backed monopole antenna is *56*° (slightly narrower than the simulated HPBW) and a shift in the maximum directivity is also observed, but predominantly this was due to fabrication and measurement setup imperfections. Nevertheless, the measured directional radiation patterns confirm the reliable radiation performance of the proposed wearable antenna.

V. Analysis of Antenna for Wearable Applications

A. *Effects of Structural Deformation*

In BAN applications, the wearable antennas are expected to be deformed or conformed during operation. Before investigating the performance in wearable scenarios, we first examined the antenna performance under structural deformation in free space to ensure its reliability. The parameters "*Rx*" and "*Ry*" are used to represent the bending radii of the antenna along the *x*-axis and *y*-axis respectively. As shown in Fig. 9(a), the assembled antenna with four different radii of curvature values, namely 15, 20, 30, and 40

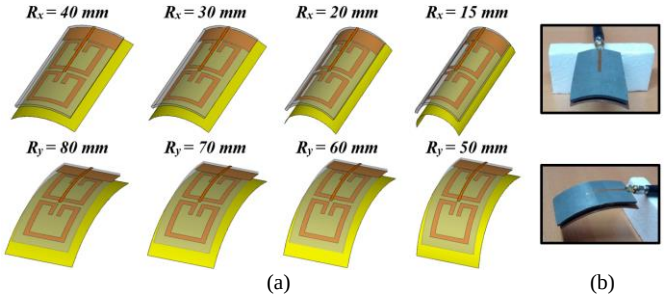

Fig. 9. (a) Structurally deformed assembled 2×1 EBG-backed monopole antenna with different values of the curvature radius, ranging from R_x = 15 mm to 40 mm along the *x*-axis and from R_y = 50 mm to 80 mm along the *y*-axis (b) Photograph of deformed antenna.

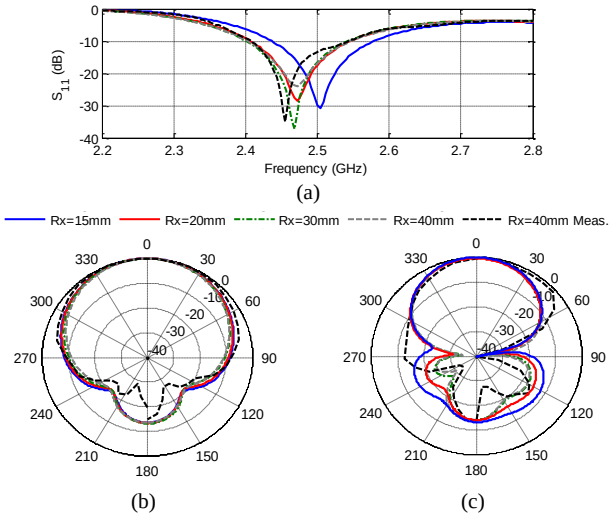

Fig. 10 (a) Simulated and measured reflection coefficient. Radiation patterns of the antenna in the (b) *y*-*z* plane and (c) *x*-*z plane* for all deformation cases in the *x*-axis.

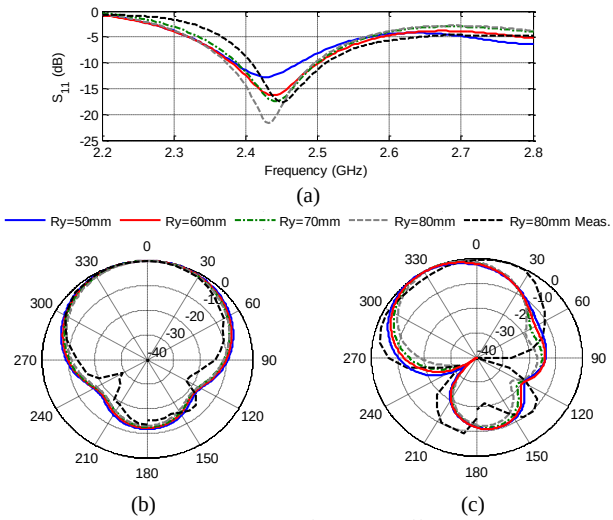

Fig. 11 (a) Simulated and measured reflection coefficient. Radiation patterns of the antenna in the (b) *y*-*z* plane and (c) *x*-*z plane* for all deformation cases in the *y*-axis.

TABLE III
COMPARISON OF GAIN AND RADIATION EFFICIENCY FOR DIFFERENT VALUES OF BENDING RADII

Bending along *x*-axis					
R_x	15	20	30	40	40 Meas.
Gain (dBi)	5.31	6.78	7.20	7.30	6.70
Radiation Efficiency	58.3%	77.8%	80.5%	78.8%	67.48%
Bending along y-axis					
R_y	50	60	70	80	80 Meas.
Gain (dBi)	5.45	6.13	6.63	6.86	6.40
Radiation Efficiency	61.0%	65.3%	69.7%	71.5%	64.1%

(mm) along the *x*-axis and 50, 60, 70 and 80 (mm) along the *y*-axis have been studied. A viably deformed fabricated prototype is also measured to confirm the accuracy of the simulation prediction as shown in Fig. 9(b). The chosen curvature radii are reasonable representations for the radii of different sizes of human arms and legs where both vertical and horizontal antenna loading is possible. Fig. 10(a) and 11(a) show the simulated and measured reflection coefficients of the antennas with the four bending radii values. As it can be seen, the resonance frequency of the antenna is well maintained below -10 dB for all selected values of R_x and R_y. In the case of the *x*-axis bending deformation, the frequency shift of less than 20 MHz can be observed when R_x is decreased from 40 to 20 mm, which is negligible. While looking at the near-extreme deformation where R_x=15 mm, a 38 MHz shift in the resonance frequency towards higher frequencies is observed. On the other hand, for the values of R_y corresponding to deformation along the *y*-axis with a decrease in the bending radius, consequent degradation of the impedance matching is observed. Particularly when R_y is decreased from 60 to 50 mm, the bandwidth decreases from 2.36–2.51 GHz when R_y = 60 mm to 2.36–2.47 GHz when R_y = 50 mm. This can be attributed to the fact that the radiated fields from the 2×1 EBG-backed monopole antenna are provided mainly by the array of EBG structures and the ground plane. The simulated and measured radiation pattern for all the cases demonstrated in Fig. 9 are presented in Fig. 10(b) and (c) for *x*-axis bending deformation and in Fig. 11(b) and (c) for *y*-axis bending deformation. The gain comparison for the same cases is summarized in Table III, confirming the high gain response of the proposed antenna even when it is deformed significantly in either the *x* or *y*-axis. The antenna efficiency is calculated based on the measured gain and simulated directivity because the measurement facility did not allow 3D radiation pattern measurements for the calculation of the measured directivity. The measured radiation patterns for the tested antennas are presented in Fig. 10 and 11 and were taken at 2.45 GHz. Because of the consistency of the simulated radiation patterns they were verified with a single measurement of the deformed antenna per axis. The measured results are in good agreement with the extensive simulation predictions and some discrepancies mostly evident in the back lobes of the antenna can be related to the measurements setup limitations. Overall, the proposed antenna performance has been shown to be robust to structural deformation along both the *x*-axis and *y*-axis and is compared favorably to several previously reported designs where degradation in impedance matching and/or significant band shifting were observed [24, 34-37].

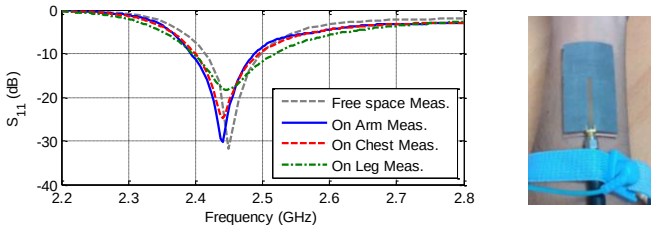

Fig. 12. Measured reflection coefficient of the assembled 2×1 EBG-backed monopole antenna placed on different parts of the human body, and a photograph of the antenna placed on the arm.

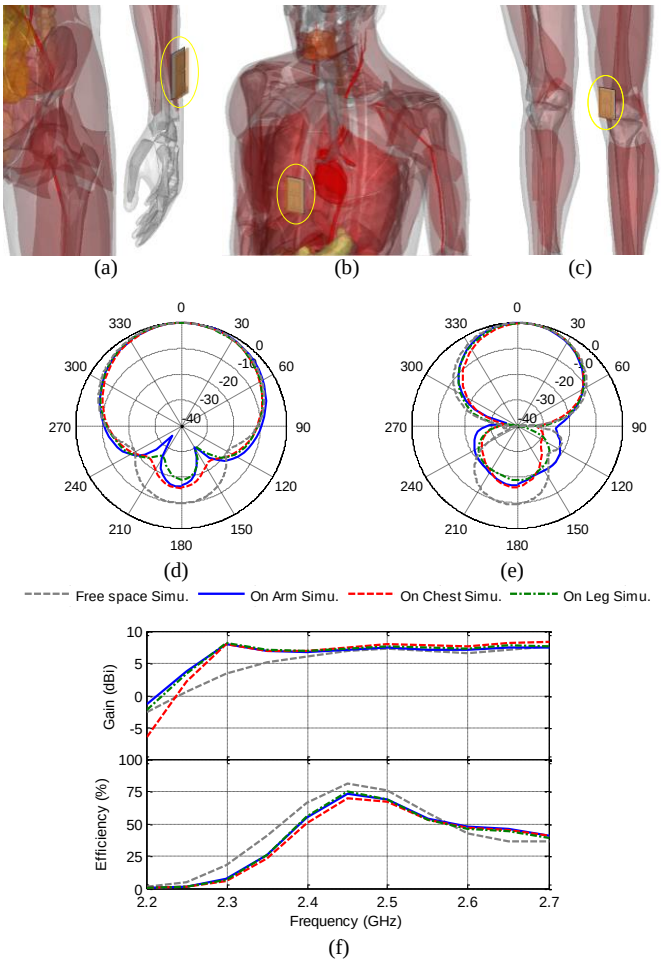

Fig. 13. 2×1 EBG-backed monopole antenna placed on the (a) arm, (b) chest and (c) leg of a realistic human body numerical phantom to evaluate the radiation characteristics presented in terms of radiation patterns at 2.45 GHz (d) along the *y*-*z* axis, (e) along the *x*-*z* axis. (f) Antenna gain and efficiency.

B. Human body loading

The EBG structure in the proposed design provides less backward radiation, hence the antenna should be tolerant to human body loading. To verify this, a series of experiments were performed where the fabricated antenna was directly placed on different parts of the body including the arm, leg and chest, while the antenna was connected to the VNA. The measured S_{11} plots presented in Fig. 12 show a very stable reflection coefficient maintained for all the measured cases of human body loading. When placed on the leg, the -10 dB bandwidth of the antenna broadens from 2.41-2.50 GHz to 2.39-2.53 GHz, where the impedance matching is still well

maintained throughout the band. A full wave EM simulation with detailed realistic human body phantom [38-39] was used to evaluate the radiation performance of the antenna when operating in close proximity to the human body. To match the measurement cases presented in Fig. 12, the antenna was placed on the arm, chest and leg of a numerical phantom as presented in Fig. 13(a) to (c). After readjusting the on-body antenna orientation the simulated radiation patterns are compared to the measurements presented in Fig. 5(a) and (b). In addition, the simulated radiation patterns, gain and efficiency for all the cases is presented in Fig. 13(d) to (f) respectively. It is evident that the front-to-back ratio of antenna for all three cases increases because the body behaves as an extension of the ground plane and it directs the radiation away from the body. This increase in directivity impacted directly the peak gain of the antenna. The efficiency of the antenna remained above 70% and the gain of antenna remained within the range of 7.07 to 7.43 dBi for all human body loading cases.

C. *Specific Absorption Rate (SAR) analysis*

Since the human body is always in the near-field of the wearable antenna, it is critical to pay adequate attention to the amount of radiation entering the human body. Near-field non-radiated power is stored around a radiating antenna and most of the energy produced in any lossy material residing close to an antenna is due to its reactive near fields. Similar conclusions have been drawn in a recent study [37]. Despite the fact that the proposed antenna operates at a comparatively narrow frequency band, having thus lower near field power density, the reactive near field is still a major contributor to the SAR. According to the FCC specifications, SAR values must be no greater than 1.6 W/kg averaged over 1 g of tissue. The SAR evaluation setup in this work consists of a simplified single-layer phantom mimicking the muscle tissue characteristics [6]. The size of the phantom is 400×400×80 mm^3, large enough to ensure $\lambda/4$ margin between antenna and phantom edges. Two SAR observation planes were introduced across the phantom box in *x-z* and *y-z* planes in the near field region for the SAR (see Fig. 14). The feeding structure of the antenna is a coaxial cable with an excitation port at its end, and the antenna is placed 2 mm above the phantom. For an input power of 0.5 W (rms), the SAR value is observed to be 0.244 W/kg averaged over 1 g of tissue, which falls well within the FCC specifications. It was demonstrated in a study performed in [16] that the SAR of the antenna can be directly controlled by increasing the size of the ground plane. A similar evaluation of the proposed antenna was performed in which the ground dimensions $G_l \times G_w$ were varied to further decrease the SAR value. An identical environment in terms of operating frequency, phantom size, phantom structure, feeding, and position of the antenna was used and the SAR was estimated over the observation planes shown in Fig. 15. When the ground dimensions $G_l \times G_w$ were increased from 68×38 mm^2 to 78×48 mm^2 (144%) and 88×58 mm^2 (197%) respectively, while keeping all other parameters constant, a significant drop in SAR was observed, as can be witnessed from the 2D plots on the observation planes shown in Fig. 15 (a) and (b). Note that all observation planes are uniformly color coded from 0 to 0.5 W/kg. It was discussed previously in sections I and II how the grounded EBG plane directs the radiation of the antenna towards the positive *z*-axis, however some of the diffracted fields from the edges of the ground plane were still seen to radiate towards the body. This effect can be controlled by increasing further the dimensions of the ground plane, giving an additional control parameter to the proposed antenna over the SAR. In conclusion, whenever it is possible, and allowed by the application, the size of the ground plane backing the EBG should be increased to further decrease the maximum SAR.

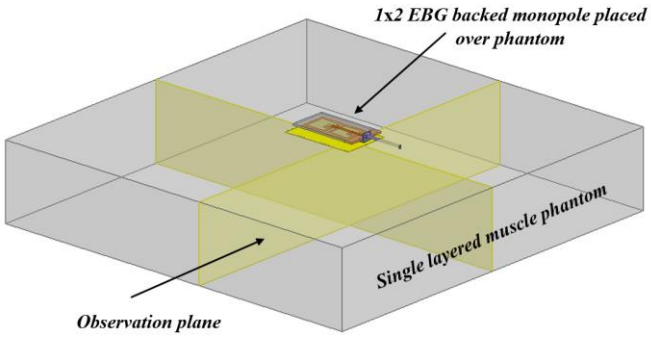

Fig. 14. Single-layer phantom for SAR computation and 2×1 EBG-backed monopole mounted on top of it.

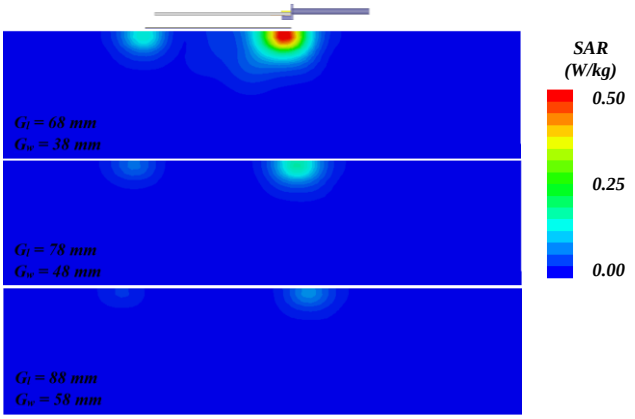

(a)

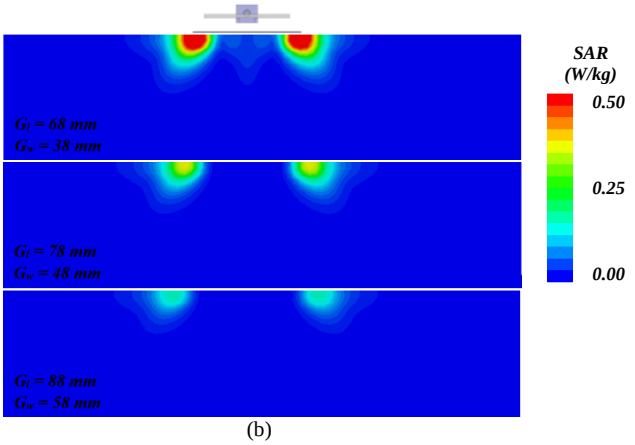

(b)

Fig. 15. SAR evaluation comparison for the 2×1 EBG-backed monopole with extensions in the ground plane (a) along *x-z* evaluation plane (b) along *y-z* evaluation plane [all the plots are averaged to the maximum value of 0.5 W/kg].

TABLE IV
COMPARISON OF PROPOSED COMPACT ANTENNA WITH EBG OR AMC BACKED PLANAR ANTENNAS

Ref.	Dimensions (mm)	Bandwidth	Max gain (dBi)	Size comparison
[37]	150×150	1.8 GHz (10.92%) 2.45 GHz (5.08%)	-	870.7%
[24]	120×120	2.45 GHz (4%) 5.50 GHz (16%)	6.4, 7.6	557.3%
[7, 23]	127×87	2.45 GHz (4.08%)	0.86	553.4%
[36]	110×130	2.45 GHz (6.18%)	-	427.6%
[31]	100×100	2.45 GHz (12%) 5.50 GHz(16.3)	2.5, 4.0	386.9%
[22]	65.7×65.7	2.45 GHz (18%)	4.8	167%
[6]	62×42	2.40 GHz (4.63%)	6.2	100.7%
This work	68×38	2.45 GHz (4.88%)	6.88	100%

VI. CONCLUSION

A compact semi-flexible 2×1 EBG-backed planar monopole antenna for wearable applications has been proposed and tested experimentally. The proposed antenna exhibits very good size and gain characteristics compared to most recently reported configurations listed in Table IV, which are intended for wearable applications. The EBG array in the proposed structure not only serves to isolate the antenna from the human body, but also contributes towards enhanced radiation efficiency. The fabricated antenna performs in good agreement with the simulated structure. It has a 4.8%, −10 dB, fractional bandwidth at the ISM band and a measured gain of 6.88 dBi, far greater than the gain of a conventional planar monopole antenna. The measured radiation pattern characteristics have been qualitatively explained using an eight-element array model consisting of six magnetic current sources and two electric current sources. Full-wave simulations and experimental measurements further revealed the robustness of the antenna to structural deformation and human body loading effects. The metallic sheet backing the EBG structure not only greatly reduces the SAR levels inside the body, but also provides direct control of its peak value. This, in addition to its low-weight, compact dimensions and ease in fabrication makes the proposed antenna very well suited for body-worn applications where the antenna can be integrated with systems for wearable biosensors or medical monitoring.

ACKNOWLEDGMENT

This research work was supported in part by the Erasmus Mundus INTACT Doctorate Level Mobility program, funded by the European Union. The authors also wish to acknowledge the Idvorski Laboratories, Belgrade, Serbia for assisting in measurements and COST Action Number IC1102 Versatile, Integrated, and Signal-aware Technologies for Antennas (VISTA) for Short-Term-Scientific-Mission grant.

REFERENCES

[1] P. S. Hall and Y. Hao, *Antenna and Propagation for Body-Centric Wireless Communications*, Norwood, MA, USA: Artech House, 2012.

[2] C. Roblin, et al. "Antenna design and channel modeling in the BAN context—part I: antennas." in *Annals of Telecommunications*, vol. 66, no. 3, pp. 139-155, Jan. 2011.

[3] Federal Communications Commission Office of Engineering, and Technology, Washington, DC, USA, "Evaluating compliance with FCC guidelines for human exposure to radiofrequency electromagnetic fields," Supplement C, 2001.

[4] M. Karimyian-Mohammadabadi, M.A. Dorostkar, F. Shokuohi, M. Shanbeh & A. Torkan, "Super-wideband textile fractal antenna for wireless body area networks." *Journal of Electromagnetic Waves and Applications*, vol. 29, no. 13, pp. 1728-1740, Jul. 2015.

[5] W. El Hajj, C. Person and J. Wiart, "A Novel Investigation of a Broadband Integrated Inverted-F Antenna Design; Application for Wearable Antenna," in *IEEE Transactions on Antennas and Propagation*, vol. 62, no. 7, pp. 3843-3846, Jul. 2014.

[6] Z. H. Jiang, D. E. Brocker, P. E. Sieber and D. H. Werner, "A Compact, Low-Profile Metasurface-Enabled Antenna for Wearable Medical Body-Area Network Devices," in *IEEE Transactions on Antennas and Propagation*, vol. 62, no. 8, pp. 4021-4030, Aug. 2014.

[7] S. Kim, Y. J. Ren, H. Lee, A. Rida, S. Nikolaou and M. M. Tentzeris, "Monopole Antenna With Inkjet-Printed EBG Array on Paper Substrate for Wearable Applications," in *IEEE Antennas and Wireless Propagation Letters*, vol. 11, pp. 663-666, 2012.

[8] L. A. Yimdjo Poffelie, P. J. Soh, S. Yan and G. A. E. Vandenbosch, "A High-Fidelity All-Textile UWB Antenna With Low Back Radiation for Off-Body WBAN Applications," in *IEEE Transactions on Antennas and Propagation*, vol. 64, no. 2, pp. 757-760, Feb. 2016.

[9] S. Yan, P. J. Soh and G. A. E. Vandenbosch, "Wearable Dual-Band Magneto-Electric Dipole Antenna for WBAN/WLAN Applications," in *IEEE Transactions on Antennas and Propagation*, vol. 63, no. 9, pp. 4165-4169, Sep. 2015.

[10] S. Agneessens and H. Rogier, "Compact Half Diamond Dual-Band Textile HMSIW On-Body Antenna," in *IEEE Transactions on Antennas and Propagation*, vol. 62, no. 5, pp. 2374-2381, May 2014.

[11] S. Yun, D. Y. Kim and S. Nam, "Folded Cavity-Backed Crossed-Slot Antenna," in *IEEE Antennas and Wireless Propagation Letters*, vol. 14, pp. 36-39, 2015.

[12] S. I. Mitu Sheikh, W. Abu-Al-Saud, and A. B. Numan, "Directive Stacked Patch Antenna for UWB Applications," *International Journal of Antennas and Propagation*, vol. 2013, Article ID 389571, 6 pages, 2013.

[13] P. B. Samal, P. J. Soh and G. A. E. Vandenbosch, "UWB All-Textile Antenna With Full Ground Plane for Off-Body WBAN Communications," in *IEEE Transactions on Antennas and Propagation*, vol. 62, no. 1, pp. 102-108, Jan. 2014.

[14] S. Yan, P. J. Soh and G. A. E. Vandenbosch, "Dual-Band Textile MIMO Antenna Based on Substrate-Integrated Waveguide (SIW) Technology," in *IEEE Transactions on Antennas and Propagation*, vol. 63, no. 11, pp. 4640-4647, Nov. 2015.

[15] S. Chamaani and A. Akbarpour, "Miniaturized Dual-Band Omnidirectional Antenna for Body Area Network Basestations," in *IEEE Antennas and Wireless Propagation Letters*, vol. 14, pp. 1722-1725, 2015.

[16] J. Trajkovikj and A. K. Skrivervik, "Diminishing SAR for Wearable UHF Antennas," in *IEEE Antennas and Wireless Propagation Letters*, vol. 14, pp. 1530-1533, 2015.

[17] M. Koohestani, J. F. Zurcher, A. A. Moreira and A. K. Skrivervik, "A Novel, Low-Profile, Vertically-Polarized UWB Antenna for WBAN," in *IEEE Transactions on Antennas and Propagation*, vol. 62, no. 4, pp. 1888-1894, Apr. 2014.

[18] Z. H. Jiang and D. H. Werner, "A Compact, Wideband Circularly Polarized Co-designed Filtering Antenna and Its Application for Wearable Devices With Low SAR," in *IEEE Transactions on Antennas and Propagation*, vol. 63, no. 9, pp. 3808-3818, Sep. 2015.

[19] Z. H. Jiang, M. D. Gregory and D. H. Werner, "Design and Experimental Investigation of a Compact Circularly Polarized Integrated Filtering Antenna for Wearable Biotelemetric Devices," in *IEEE Transactions on Biomedical Circuits and Systems*, vol. 10, no. 2, pp. 328-338, Apr. 2016.

[20] N. M. Mohamed-Hicho, E. Antonino-Daviu, M. Cabedo-Fabrés, M. Ferrando-Bataller and D. Sanchez-Escuderos, "Wideband high-impedance surface reflector for low-profile high-gain UHF antenna," *2015 9th European Conference on Antennas and Propagation (EuCAP)*, Lisbon, 2015, pp. 1-4.

[21] O. Folayan and R. Langley, "Dual frequency band antenna combined with a high impedance band gap surface," in *IET Microwaves, Antennas & Propagation*, vol. 3, no. 7, pp. 1118-1126, Oct. 2009.
[22] H. R. Raad, A. I. Abbosh, H. M. Al-Rizzo and D. G. Rucker, "Flexible and Compact AMC Based Antenna for Telemedicine Applications," in *IEEE Transactions on Antennas and Propagation*, vol. 61, no. 2, pp. 524-531, Feb. 2013.
[23] S. Kim, M. M. Tentzeris and S. Nikolaou, "Wearable biomonitoring monopole antennas using inkjet printed electromagnetic band gap structures," *2012 6th European Conference on Antennas and Propagation (EUCAP)*, Prague, 2012, pp. 181-184.
[24] S. Zhu and R. Langley, "Dual-Band Wearable Textile Antenna on an EBG Substrate," in *IEEE Transactions on Antennas and Propagation*, vol. 57, no. 4, pp. 926-935, Apr. 2009.
[25] R. Marques, F. Martin, and M. Sorolla, Metamaterials with Negative Parameters. New York: Wiley, 2007.
[26] M. Tang, S. Xiao, T. Deng and B. Wang, "Novel folded single split ring resonator and its application to eliminate scan blindness in infinite phased array," *2010 International Symposium on Signals Systems and Electronics (ISSSE)*, , Nanjing, 2010, pp. 1-4.
[27] G. V. Eleftheriades and K. G. Balmain, *Negative-refraction metamaterials: fundamental principles and applications*. John Wiley & Sons, 2005.
[28] F. Yang and Y. Rahmat-Samii, "Reflection phase characterizations of the EBG ground plane for low profile wire antenna applications," in *IEEE Transactions on Antennas and Propagation*, vol. 51, no. 10, pp. 2691-2703, Oct. 2003.
[29] L. Akhoondzadeh-Asl, D. J. Kern, P. S. Hall and D. H. Werner, "Wideband Dipoles on Electromagnetic Bandgap Ground Planes," in *IEEE Transactions on Antennas and Propagation*, vol. 55, no. 9, pp. 2426-2434, Sep. 2007.
[30] F. Yang, A. Amir, and Y. Rahmat-Samii. "A novel surface-wave antenna design using a thin periodically loaded ground plane," *Microwave and Optical Technology Letters*, vol. 47, pp. 240–245, 2005.
[31] S. Yan, P. J. Soh and G. A. E. Vandenbosch, "Low-Profile Dual-Band Textile Antenna With Artificial Magnetic Conductor Plane," in *IEEE Transactions on Antennas and Propagation*, vol. 62, no. 12, pp. 6487-6490, Dec. 2014.
[32] H. Mosallaei and K. Sarabandi, "Antenna miniaturization and bandwidth enhancement using a reactive impedance substrate," in *IEEE Transactions on Antennas and Propagation*, vol. 52, no. 9, pp. 2403-2414, Sep. 2004.
[33] S. Nikolaou et al., "Pattern and frequency reconfigurable annular slot antenna using PIN diodes," in *IEEE Transactions on Antennas and Propagation*, vol. 54, no. 2, pp. 439-448, Feb. 2006.
[34] E. F. Sundarsingh, S. Velan, M. Kanagasabai, A. K. Sarma, C. Raviteja and M. G. N. Alsath, "Polygon-Shaped Slotted Dual-Band Antenna for Wearable Applications," in *IEEE Antennas and Wireless Propagation Letters*, vol. 13, pp. 611-614, 2014.
[35] B. Hu, G. P. Gao, L. L. He, X. D. Cong and J. N. Zhao, "Bending and On-Arm Effects on a Wearable Antenna for 2.45 GHz Body Area Network," in *IEEE Antennas and Wireless Propagation Letters*, vol. 15, pp. 378-381, 2016.
[36] P. Salonen and Y. Rahimat-Samii, "Textile antennas: effects of antenna bending on input matching and impedance bandwidth," in *IEEE Aerospace and Electronic Systems Magazine*, vol. 22, no. 3, pp. 10-14, Mar. 2007.
[37] S. Velan *et al*., "Dual-Band EBG Integrated Monopole Antenna Deploying Fractal Geometry for Wearable Applications," in *IEEE Antennas and Wireless Propagation Letters*, vol. 14, pp. 249-252, 2015.
[38] E. Y. Chow, M. M. Morris and P. P. Irazoqui, "Implantable RF Medical Devices: The Benefits of High-Speed Communication and Much Greater Communication Distances in Biomedical Applications," in *IEEE Microwave Magazine*, vol. 14, no. 4, pp. 64-73, Jun. 2013.
[39] M. A. B. Abbasi, D. Philippou, and S. Nikolaou, "Comparison Study of Layered Homogeneous Models with Detailed Human Tissue Models for Through-body Communications," in *Progress in Electromagnetics Research Proceedings*, Prague, Jul. 2015, pp. 1796 - 1799.
[40] T. Tuovinen, M. Berg, K. Y. Yazdandoost, E. Salonen and J. Iinatti, "Reactive near-field region radiation of planar UWB antennas close to a dispersive tissue model," *2012 Loughborough Antennas and Propagation Conference (LAPC)*, , Loughborough, UK, Nov. 2012, pp. 1-4.
[41] G. Kumar and K. P. Ray, *Broadband Microstrip Antennas*. Norwood, MA: Artech house, 2003.
[42] R. Garg, et al., *Microstrip Antenna Design Handbook*, Norwood, MA: Artech House, 2001.
[43] C. A. Balanis, *Antenna Theory Analysis and Design*, New York: John Wiley & Sons, 1997.

M. Ali Babar Abbasi (M'14) received the B.S. degree in electrical (telecommunication) engineering from COMSATS Institute of Information Technology, Islamabad, Pakistan, in 2011 and the MS degree in electrical engineering from National University of Sciences and Technology Islamabad, Pakistan, in 2013. Currently he is working toward the Ph.D. degree in electrical engineering (focusing on applied electromagnetics) at the Frederick University, Nicosia, Cyprus.

He has authored or coauthored more than 15 publications in peer-reviewed journals and conferences. His research interests include passive and active antennas for biomedical devices, wireless sensors, and reconfigurable RF electronics.

Mr. Abbasi was a recipient of the Erasmus Mundus INTACT Doctoral scholarship by Europian Union in 2014, and the COST VISTA short-term Scientific Mission (STSM) grant, in 2016. Mr. Abbasi, was also the finalist in Ericsson Innovation Awards 2016, and the regional winner of IET Presentation Around the World (PATW) in 2016.

Symeon (Simos) Nikolaou (M'08) received the B.S.E.C.E. degree from the National Technical University of Greece (NTUA) Athens, Greece, in 2003 and the M.S.E.C.E. and Ph.D. degrees from the Georgia Institute of Technology (GaTech), Atlanta, in 2005 and 2007, respectively.

In September 2007, he joined the faculty of Electrical Engineering at Frederick University, Nicosia Cyprus where he is currently an Assistant Professor. He has authored or co-authored more than 50 publications in peer reviewed journals and conferences. His research interests include the design of UWB, conformal and reconfigurable antennas, wearable and implantable devices, RFIDs and wireless sensors, wireless power charging, and reconfigurable filters.

Marco A. Antoniades received the B.A.Sc. degree in electrical engineering from the University of Waterloo, ON, Canada, in 2001, and the M.A.Sc. and Ph.D. degrees in electrical engineering from the University of Toronto, ON, Canada, in 2003 and 2009, respectively.

He is a Lecturer in the Department of Electrical and Computer Engineering at the University of Cyprus, and an Adjunct Fellow in the School of Information Technology and Electrical Engineering at The University of Queensland, Australia. He has authored over 65 refereed publications, and has coauthored three book chapters titled Transmission-Line Based Metamaterials in Antenna Engineering that appears in the Handbook of Antenna Technology (Springer Science, 2015), Antenna Applications of Negative Refractive Index Transmission-Line (NRI-TL) Metamaterials that appears in the Modern Antenna Handbook (Wiley, 2008) and Compact Planar Multiband Antennas for Mobile Applications that appears in Advancements in Microstrip and Printed Antennas (InTech, 2013). His research interests include passive and active antenna design, RF/microwave circuits and negative-refractive-index metamaterials for use in broadband wireless communications, biomedical devices and imaging, space/satellite applications, radio-frequency identification, and wireless power transfer.

Dr. Antoniades received the Hellenic Canadian Federation of Ontario Academic Excellence Award in 2003, and the Edward S. Rogers Sr. Graduate Scholarship from the University of Toronto during 2003–2004 and 2004¬–2005. He also received the First Prize in the Student Paper Competition at the 2006 IEEE AP-S International Symposium on Antennas and Propagation. During 2009–2011, he was the recipient of the Ontario Post-Doctoral Fellowship from the Ministry of Research and Innovation of Ontario. He has served as the joint conference chair for the 2015 Loughborough Antennas and Propagation Conference (LAPC), on the steering committee for the 2010 IEEE AP-S International Symposium on Antennas and Propagation, and

serves regularly on the technical program committee for the IEEE AP-S International Symposium on Antennas and Propagation (APS/URSI), the European Conference on Antennas and Propagation (EuCAP), and the IEEE Radio and Wireless Symposium (RWS). He currently serves as a member of the IEEE AP-S Education Committee and is an associate editor for IET Microwaves, Antennas and Propagation (MAP).

Marija Nikolić Stevanović received the B.Sc., M.Sc. and Ph.D. degrees from University of Belgrade in 2000, 2003, and 2007, respectively. In 2001, she joined the School of Electrical Engineering, University of Belgrade as a Teaching assistant. In 2008 she was promoted to an Assistant professor. In 2011, she obtained the Ph.D. degree in electrical engineering from Washington University in St. Louis, USA. She is interested in inverse scattering, array processing, and antennas analysis and design.

Dr. Photos Vryonides received the Diploma, M.Phil and Ph.D. degrees in Electrical and Electronic Engineering from the University of Manchester Institute of Science and Technology (UMIST), UK, in 1998, 1999, and 2002 respectively. Since 2007 he is tenured track faculty member at Frederick University and senior researcher at Frederick Research Center (FRC). Dr. Vryonides is member of the Antennas and Microwaves research group and his research interests span: mixers, LNAs, PAs, broadband amplifiers, millimetre-wave couplers, reconfigurable microwave filters, low phase noise oscillators and millimetre-wave MMIC design and components. Photos has authored or co-authored more than 40 papers in journals and peer reviewed conferences.